Chapter 3

Experimental techniques

Sp-STM investigations are best performed on well-defined, stable and reproducible surfaces. Thus, all Sp-STM experiments were performed in ultra high vacuum (UHV). The experimental equipment used for the investigations is presented in the following. A detailed description of the performance of the Sp-STM is given including the design of Sp-STM ring electrodes. To test the extension of the Sp-STM to measure a well-defined in-plane component, measurements are shown which were performed on a well-studied system, a 180° domain wall at the surface of Fe-whiskers.

3.1 Equipment

The experimental setup is the one that has been used now for several years to measure the out-of-plane component of the spin polarization with the Sp-STM. All Sp-STM measurements were performed in an UHV chamber with a base pressure of $1*10^{-10}$ mbar. The whole equipment consists of a three chamber system (air-lock, load-lock, main chamber) each having its own pumps. They are separated by valves and equipped with a transfer mechanism for samples and electrodes. This allows a transfer of STM-electrodes and samples from ambient conditions into the main chamber within 3 hours without breaking the vacuum. To avoid intense degassing of new samples and electrodes in the main chamber, baking can take place in each of the chambers. Since STM measurements are sensitive to all kind of mechanical vibrations, the whole chamber system sits on a pneumatic suspension system.

The main chamber consists of two parts, the preparation chamber and the STM chamber. The preparation chamber is equipped with a sputtering gun, an Auger electron spectrometer (AES), a low energy electron diffractometer (LEED), evaporators for the deposition of materials, and a Kerr-microscope. Fig. 3.1 shows an image of the whole vacuum system where the main facilities are indicated.

The differentially pumped sputter gun is used to clean sample surfaces by Argon ion bombardment. Surface atoms are removed by the impact of Argon ions having energies between 1 and 3 keV. Because the ion bombardment destroys the crystal

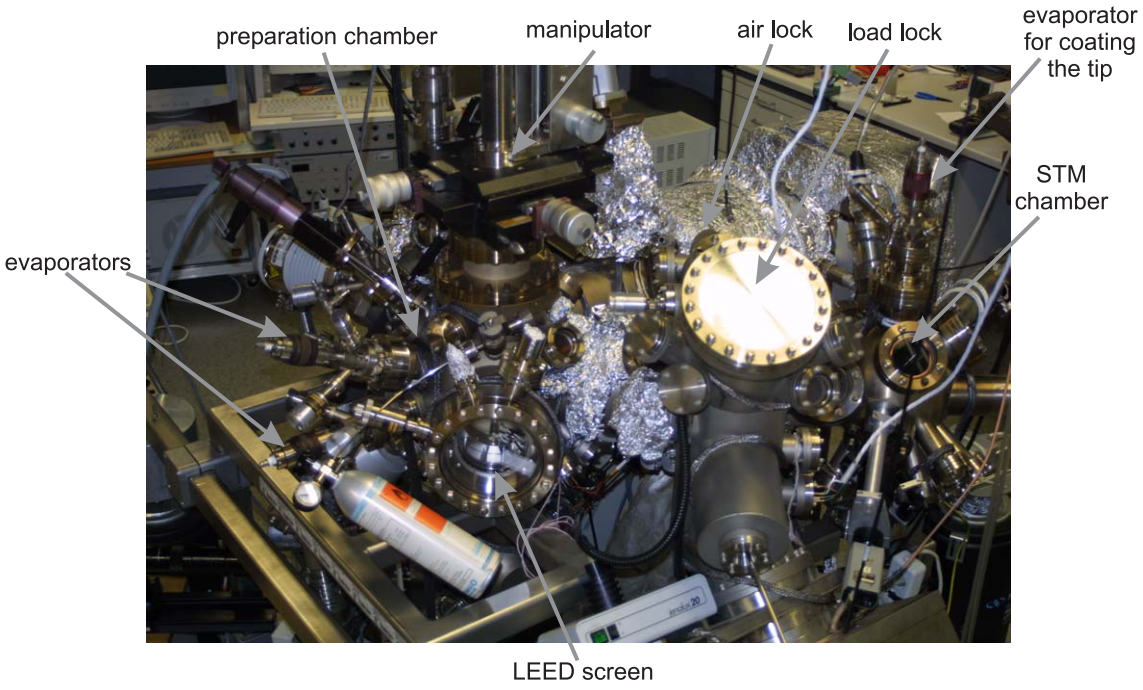

Figure 3.1: Image of the experimental UHV-chambers. The main features are indicated in the image.

lattice structure at the sample surface, the crystals were annealed after sputtering to reduce the induced defects and to release the implanted Ar.

AES allows the characterization of chemical elements at the sample surface. Auger electrons give information of the top most layers, up to about 15 layers depending on the energy of the Auger electrons. The chemical sensitivity is achieved because Auger electron energies are determined by the transition energies between core level electron states which are element specific.

To study the crystalline structure of the sample surface, LEED was used. Because of the low kinetic energy (up to 200 eV) of the incoming electrons the penetration depth without energy loss is only a few atomic layers. In LEED the diffraction of electrons with wave length of a few Å is used to create a diffraction pattern of the two dimensional reciprocal lattice of the sample surface. In the case of a single domain surface this pattern can be transformed into real space showing the unit cell of the crystal structure at the sample surface. LEED is mainly sensitive to periodic structures.

The evaporators are used to thermally evaporate a material onto a substrate by molecular beam epitaxy. This method allows the growth of well-defined films from the sub monolayer range up to nanometer thickness.

The LEED screen and the AES gun are positioned opposite to each other. This configuration is used for medium energy electron diffraction (MEED) measurements where the AES electron gun supplies the medium energy electrons (about 5 keV) and

the diffraction pattern is displayed on the LEED screen. MEED is performed during the evaporation of a material to a substrate. In the case of layer-by-layer growth the amount of deposited material can be determined by ML period oscillations of the diffraction spots.

The Kerr effect exploits the change of polarization of light upon reflection from magnetic surfaces. Linear polarized light can be separated into left and right circular polarized light. The reflection coefficient of magnetic surfaces is different for left and right circular polarized light. It depends on the relative orientation of the magnetization and the electrical polarization[1]. In general, incident linear polarized light is elliptically polarized with a rotated polarization plane after reflected from a magnetic surface. The change of the polarization state of the light is measured by the Kerr-ellipticity and the Kerr-rotation. A Kerr-effect setup consists of a light source, a polarizer, an analyzer, and a detector. In our case, we use light coming from a halogen lamp. The light beam passes a bandpass filter and the polarizer before it is reflected from the surface. The reflected light passes an analyzer and is imaged with a CCD-camera. Kerr measurements were performed in the longitudinal geometry which means that the magnetization of the sample lies in the scattering plane of the light. One can increase the Kerr contrast by calculating the asymmetries[2]. This procedure exploits the fact that the Kerr signal has a reversed sign on both sides of the extinction whereas changes due to the surface topology do not.

3.1.1 The spin-polarized scanning tunneling microscope

For the experiments, we used a commercially available Omicron μ-STM [88]. Care was taken to avoid any magnetic material in the sample stage of the STM to exclude an influence on the spin sensitive measurements. The electrical circuit of the Sp-STM is schematically shown in Fig. 3.2. The voltage applied between the sample and the ring is called U_{gap}. The measurements were performed in the constant current mode (see section 2.2), where the tunneling current is controlled by the feedback loop with a cut-off frequency $f_{control}$. In this loop, variations of the tunneling current are compensated by changes of the distance between ring and sample by changes of the voltage of the z-piezo. The change of the z-piezo voltage can be recorded which results in the topographic image. With a lock-in amplifier an alternating current of frequency f_{mod} between 15 to 30 kHz is applied to the coil around the ring to switch its magnetization. Because of the dependence of the tunneling current on the relative orientation of the magnetization between the ring and sample this results in a modulation of the tunneling current. By choosing $f_{mod} \gg f_{control}$ the feedback loop collects the average tunneling current. It contains no information on the spin

[1]The electrical polarization $\mathrm{Pe_i}$ is defined by $\mathrm{Pe_i} = \chi_{\mathrm{ij}}\mathrm{E_j}$ for small electrical fields (E). χ is the electrical susceptibility. For details see Ref. [87].

[2]For the asymmetry, two Kerr images were taken for analyzer positions on both sides of the extinction (some mrad). The asymmetry is then defined as the difference of the two Kerr images divided by the sum of them.

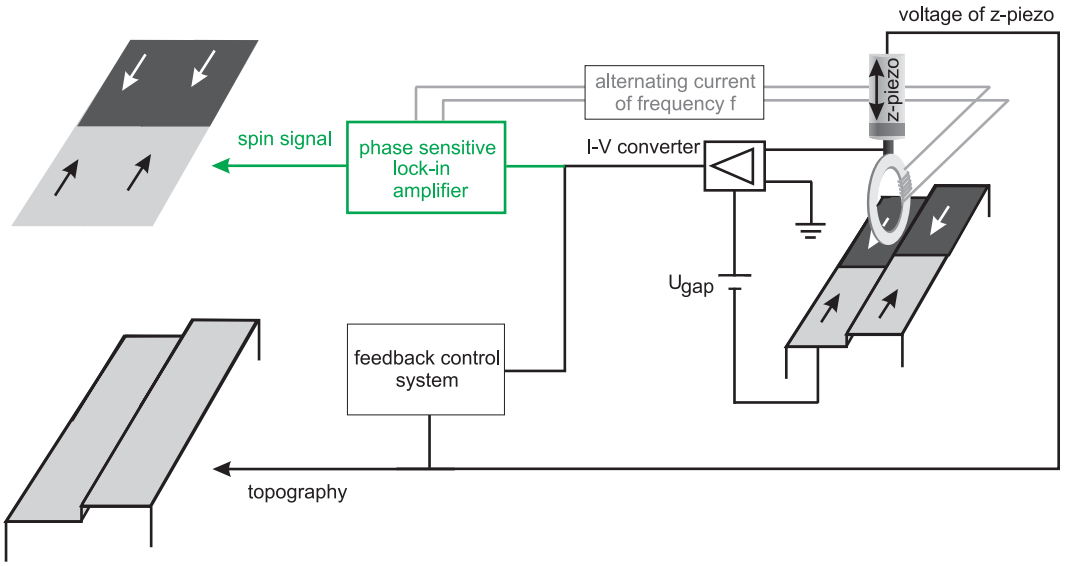

Figure 3.2: Electric circuit of the Sp-STM with the separation of topography and spin signal.

polarization. The modulation of the tunneling current is analyzed with a phase sensitive lock-in amplifier, yielding the spin signal [4].

A sketch of the relation between the switching of the magnetization of the ring, the spin-dependent tunneling current, and the average tunneling current as a function of time is shown in Fig. 3.3. The magnetization of the ring is switched with a constant frequency. The cases a) and b) represent the spin-dependent tunneling current measured on two domains being oppositely magnetized. When the ring is crossing the domain wall, a phase shift of π occurs in the spin-dependent tunneling current which means the order between parallel and antiparallel alignment is reversed (the signal in case a) and case b) are phase shifted by π). If the magnetization of the ring is not completely collinear to the magnetization of the domains, the behavior stays the same but the amplitude ΔI decreases. By separating $\bar{I}$ and ΔI and analyzing the latter with respect to the correct phase, the topography and the spin polarization of a sample surface can be imaged at the same time. The spin signal is defined as the spin-polarized tunneling current normalized to the average tunneling current $\Delta I/\bar{I}$. The spin contrast is defined as the difference of the spin signal measured between two neighboring domains normalized to $2\bar{I}$. Because of the processing of the measured signal, the spin signal included in the spin contrast is multiplied by $2\sqrt{2}$ to obtain the true physical quantity of the current asymmetry. This allows the comparison between experimental and theoretical data, as shown later in chapter 5.

In our setup, a sinusoidal alternating current is applied to the coil. Because the phase shift between the applied current and the modulation caused in the tunneling current depends on the frequency and the impedances of all involved components,

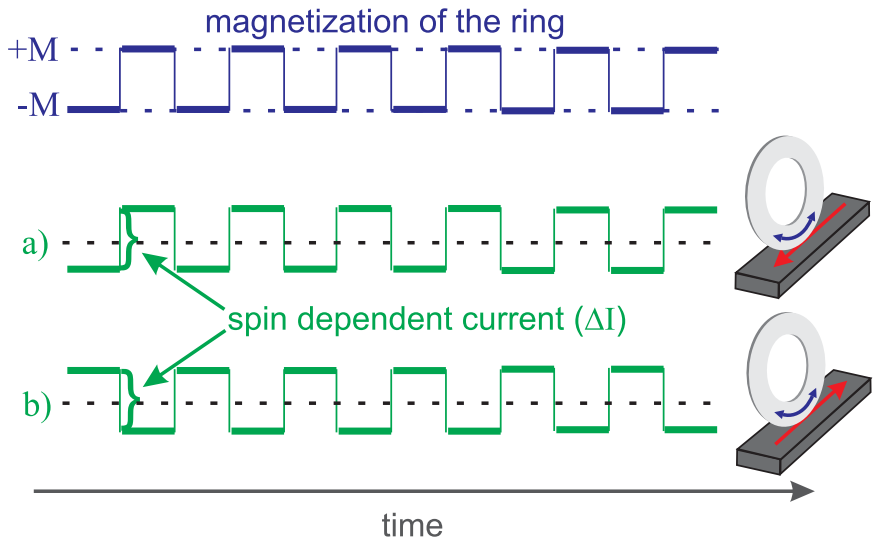

Figure 3.3: Schematic drawing of the relation between the switching of the magnetization of the Sp-STM electrode between the two saturation values $+M$ and $-M$ and the different current contributions. The black dashed lines represent the average tunneling current. Between oppositely magnetized domains, a phase shift of π occurs in the spin-dependent tunneling current, represented by case a) and b).

two lock-in signals, signal channel (1) and channel (2) having a phase shift of $\pi/2$, are measured. Therefore, the full information is measured without a-priori knowing the exact phase correlation. The maximal spin signal is given by:

$$\cos\gamma \cdot \text{signal channel}(1) - \sin\gamma \cdot \text{signal channel}(2), \tag{3.1}$$

γ being the phase. The right phase is found by determining the phase correlation γ yielding the minimal spin contrast and calculating the spin signal for $\gamma + 90°$.

Fig. 3.4 shows an image of the Sp-STM. For adjusting the sample and ring position, the STM stage is equipped with three coarse piezos for the lateral movement and one for the vertical. The scanner (Omicron scanner) with the ring on top consists of a piezo tube which controls the precise movement of the ring over the sample surface during the scanning process. To change the ring, the whole scanner is transferred out of the vacuum chamber. In addition to the commercially STM setup, two wires are connected to apply an alternating current to the coil. The STM is placed on Viton O-rings to decouple the STM from mechanical vibrations of the chamber. Additional filters in the electric circuit of the instruments suppress high frequency noise of the power lines.

The lateral calibration of the scanner was performed on the reconstruction of a Au(111) surface. The reconstruction pattern and the distance between corrugation lines was compared with measurements performed by Barth and coworkers [89] and by van Hove and coworkers [90]. The distance between the corrugation lines is 6.3 nm. Fig. 3.5 shows reconstruction patterns imaged after calibration. Clearly

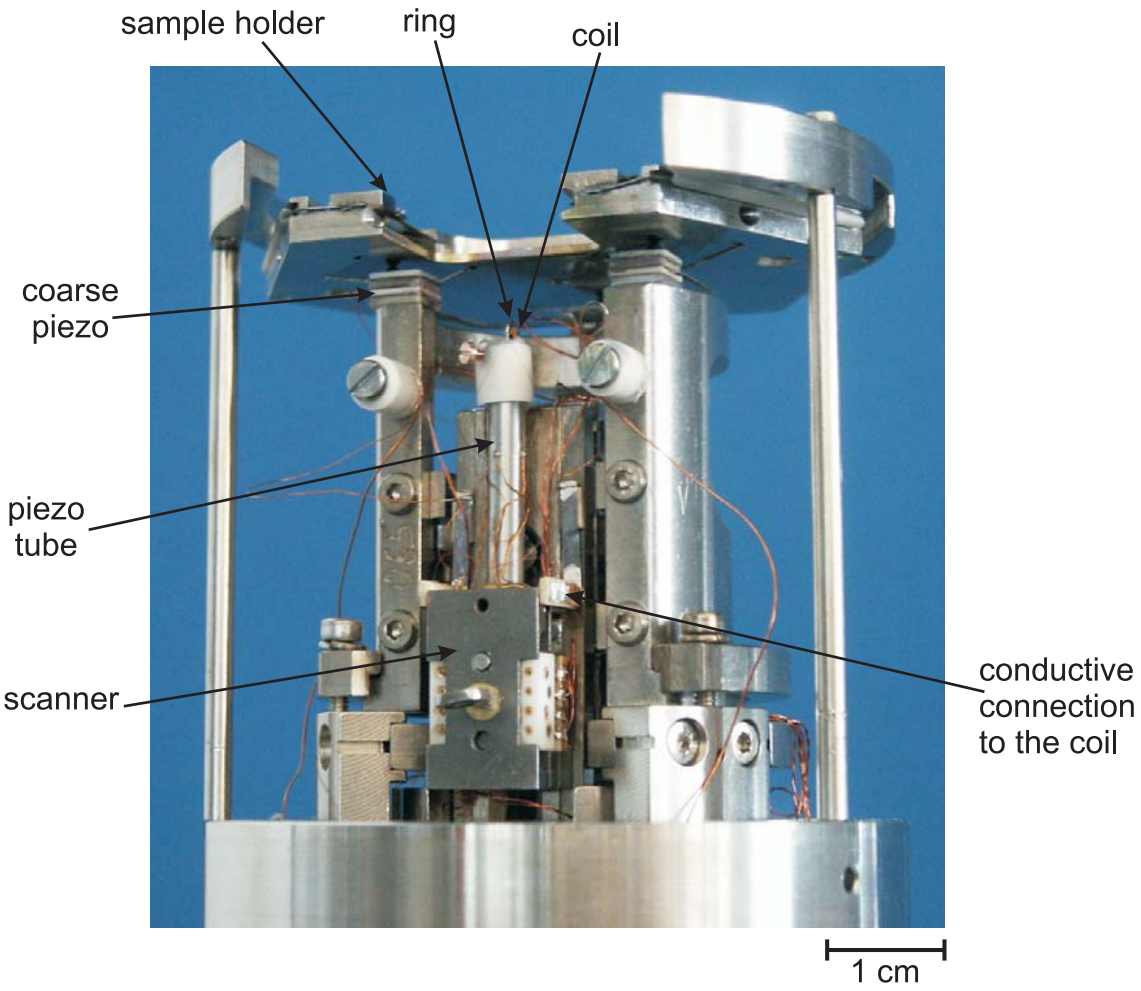

Figure 3.4: Image of the Omicron μ-STM with the modification for Sp-STM measurements.

pairwise arranged corrugation lines of the reconstruction are visible.

3.1.2 Preparation of ring electrodes

We use an amorphous alloy of $Co_{68.15}Fe_{4.35}Si_{12.5}B_{15}$ [91] for the Sp-STM electrodes. This material is commercially available. The material has a nearly vanishing magnetostriction ($< 10^{-8}$) [4], which means that nearly no changes of the shape of the material occurs during the magnetization reversal process. This is important to prevent changes of the distance between the electrode and the sample surface during the switching of the magnetization of the electrode. As a rule of thumb, a distance change of 10 pm produces a change of about 20% of the tunneling current[3]. The

[3]In first approximation one can assume that the tunneling current depends exponentially on the distance between STM electrode and sample surface [67], see section 2.2.

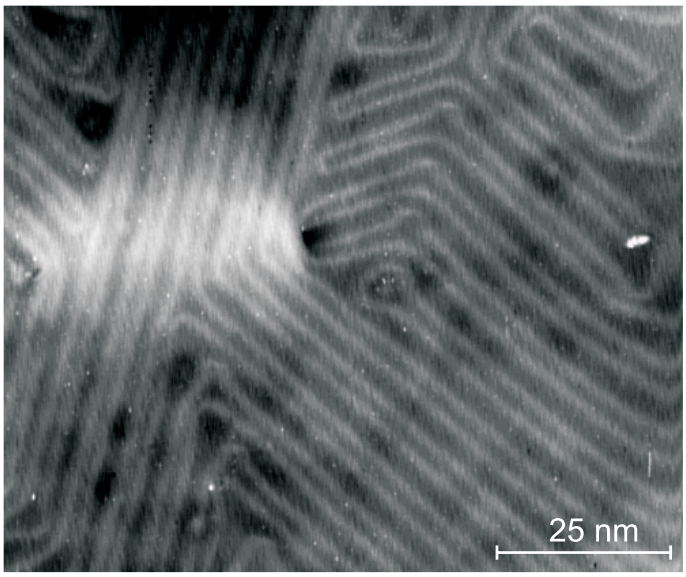

Figure 3.5: Typical reconstruction visible at the Au(111) surface, measured with STM. Pairwise arranged corrugation lines and zigzag patterns of the reconstruction are visible.

material has a low intrinsic coercitivity smaller than 10 μT. Therefore, only small magnetic fields are needed to switch the electrode magnetization. The low coercivity also results in low magnetic losses which avoids energy dissipation and thus periodic heating and thermal expansion of the electrode. This allows a rapid switching of the magnetization of the electrode without mechanical vibrations.

The rings used as Sp-STM electrodes were electrochemically etched from a foil of 25 μm thickness. To etch rings, we glued non conducting masks on one side of the CoFeSiB foil. These etching masks had an outer diameter of 2 mm and an inner diameter of 0.7 mm. Onto the other side of the foil, adhesive-tape was fixed. A schema of this preparation setup is shown in Fig. 3.6. The etching solution was a mixture of HF (40%), HCl (32%) and H_2O. One electrode was a Pt wire (cathode) and the other one was the CoFeSiB foil (anode). By applying a voltage between these two electrodes, the foil around the ring masks was etched away and rings remained on the adhesive-tape. During the etching process, a current of 40-60 mA was flowing. After etching, the masks and the adhesive-tape were removed with ethanol. The etching procedure alone produces some irregular structures at the outer perimeter of the rings, the part which was later used for scanning. To reduce the roughness, the outer perimeter of the rings was polished. The rings were polished with sand-paper of a grain size of 10 μm for 5 min, afterwards with a diamond paste, 10 min with a grain size of 6 μm, 10 min with a grain size of 1 μm and 5 min with a grain size of 0.25 μm. After these preparation steps, the rings were annealed in H_2 atmosphere to 513 K for 3 h. The ring material cannot be annealed to higher temperatures, because it crystalizes and becomes hard magnetic. Finally, a small

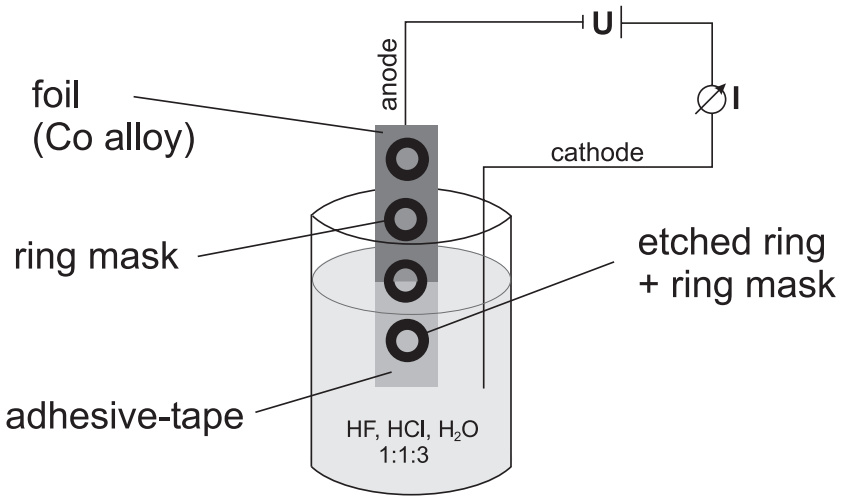

Figure 3.6: Schematic drawing of the electrochemical etching process.

coil of an insolated copper wire of 50 μm diameter was wound around the ring. The coil was fixed with a non conducting glue to avoid mechanical vibrations. To connect the ring to the STM scanner, a Ta wire was fixed to the ring with a conductive silver glue solution. In Fig. 3.7a) a photo of a ring is shown, as it is used for Sp-STM measurements. One can see the thin ring with a small coil to allow switching of the ring magnetization and the Ta wire for fixing the ring to the scanner. Just for clarification, the rings used as Sp-STM electrodes are macroscopic objects of about 2 mm in diameter and 25 μm in width. The quality of the outer perimeter of rings prepared as described above were investigated with a scanning electron microscope (SEM). Fig. 3.7b) shows an image of a part of the outer perimeter. Some grooves of some 100 nm in width could be found which originated from polishing. However, they are parallel to the outer perimeter and hence, they should not influence the tangential magnetization. A ring with an outer diameter of 2 mm is not expected to yield a high lateral resolution in STM measurements. Microscopically, there are small protrusions coming from polishing and possibly tips on the nanometer scale. Tunneling from such defects may result in a high lateral resolution. As usually in STM measurements, the exact shape of the tunneling-tip remains unknown. For Sp-STM it is on one hand essential to have a flat ring to ensure that the magnetization in the tunneling region switches in a well-defined way and on the other hand it is important to have not completely flat rings, so that a good lateral resolution is obtained.

The tip apex of a ring can be modified during STM operation by applying a high potential (about 10 V) for a short moment so that a few atoms can move from the surface to the tip apex or the other way round, depending on the sign of the bias voltage. This treatment can form a sharp tip apex. Also, a controlled crash of the tip apex into a sample surface can produce sharp nano tips [64].

To determine the current needed to switch the ring, magneto-optical Kerr-effect

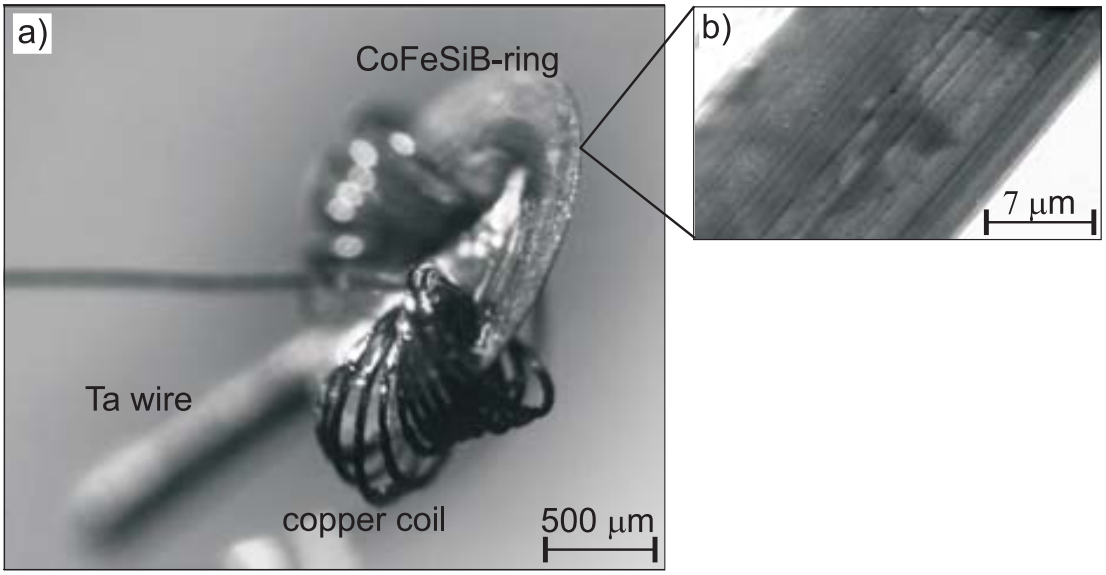

Figure 3.7: a) Optical image of a ring electrode (outer diameter: 2 mm, inner diameter: 0.7 mm) as used for Sp-STM measurements. Also visible are the coil around the ring and a connecting Ta wire. b) SEM image taken at the outer perimeter of a ring where tunneling can occur.

measurements were performed. The Kerr measurements were performed on a single spot on the ring surface. A current was applied to the coil and the ellipticity of the reflected light was measured as a function of this current. Such a Kerr loop is shown in Fig. 3.8. A small current of about 4 mA is sufficient to fully reverse the magnetization of the ring (coil with 20 turns).

After the etched ring was transferred into the vacuum, the outer perimeter, later used for tunneling, was cleaned by Argon sputtering for some hours. Before each measurement, the outer perimeter was always sputtered for some minutes. We figured out that a small amount of Fe deposited on the tunneling part of the outer perimeter improved the contrast in the spin signal. Thus, some Fe, ≈10 ML was evaporated on this part of the ring before operating Sp-STM measurements.

3.2 In-plane measurements on a test sample: Fe-whisker

We chose Fe-whiskers as test samples since they have been extensively studied in the past and are a well-defined system concerning the domain pattern, the orientation of the magnetization in domains, and the width of domain walls.

Fe-whiskers are Fe single crystal needles of bcc Fe with a lattice constant of 0.287 nm. They are grown from the vapor phase and form needles with a rectangular

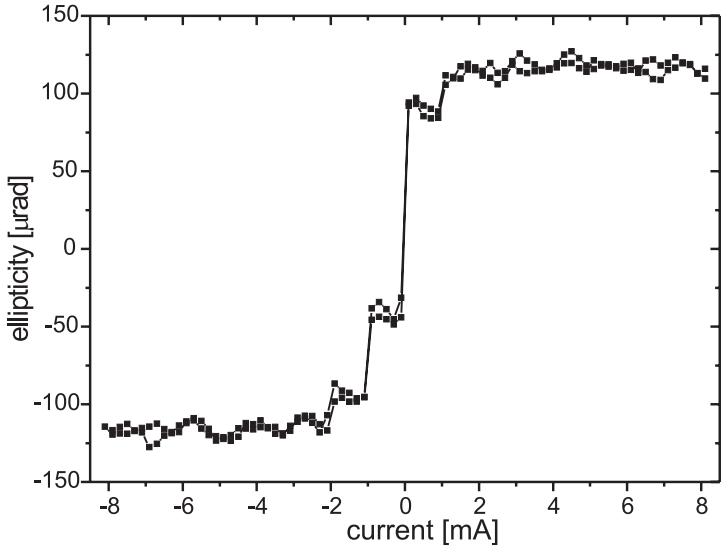

Figure 3.8: Kerr measurement performed on a ring used for Sp-STM measurements. To fully reverse the ring magnetization a current of ≈4 mA is needed for a coil with 20 turns.

cross section and a length of 1 to 2 cm [48]. To illustrate the size and shape of a typical Fe-whisker, an image taken with a scanning electron microscope shows an Fe-whisker together with a fruit fly (Fig. 3.9). Good quality Fe-whiskers have nearly perfectly flat surfaces with terraces of several 100 nm width. The long axis lies along a $\langle 100 \rangle$ crystal axis and the surfaces are formed by (100) planes. A STM image of the topography of an Fe-whisker surface (Fig. 3.9b) shows terraces of 500 nm width. Sometimes defects exist on the surface, and occasionally screw dislocations could be found (Fig. 3.9c)).

The magnetization of Fe-whiskers is in the plane of the surface with easy axes along $\langle 100 \rangle$. Fe-whiskers are magnetically soft meaning the magneto-crystalline anisotropy is much smaller than the stray field energy. Therefore, the domain structure is mainly caused by minimizing the stray field energy. The domain structure of stress free and nearly perfect Fe-whiskers is simple. In the demagnetized state, the sample is subdivided into domains. Typically, the domain pattern consists of a so-called Landau structure, where a 180° domain wall runs parallel to the long axis of the Fe-whisker and end domains which have 90° walls to close the magnetic flux at the surface (Fig. 3.10a)). 180° domain walls always lie along the $< 100 >$ direction and 90° domain walls along the $< 110 >$ direction [48]. In bulk Fe, 180° domain walls are Bloch walls in the volume of the crystal, while at the surface they form Néel caps [93] to minimize the stray field energy at the sample surface. The domain pattern has been extensively investigated with electron microscopy with polarization analysis (SEMPA) [94], Kerr-microscopy [48], and magnetic force microscopy [95].

180° domain walls of Fe-whiskers easy move in an applied external magnetic

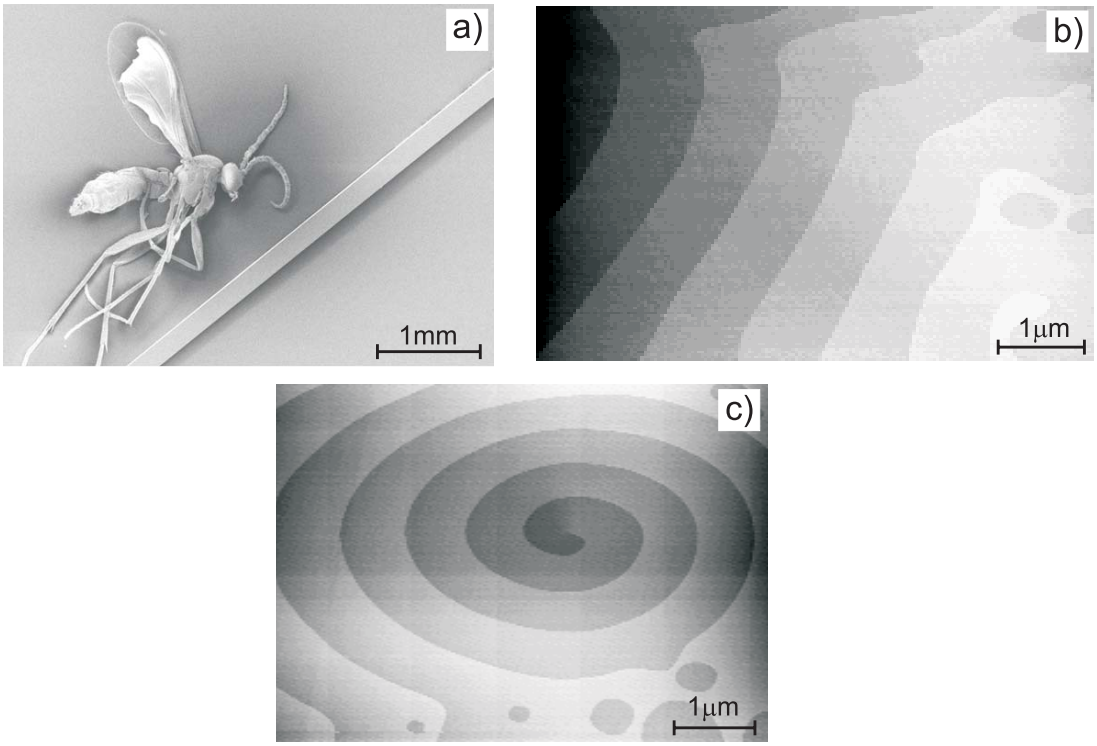

Figure 3.9: a) SEM image of an Fe-whisker. A fruit fly is also shown to illustrate the dimension of Fe-whiskers [92]. b), c) STM images of an Fe-whisker surface. The different gray scales show steps of monatomic height. A flat Fe-whisker surface with a terrace width of about 500 nm is shown in b) and a screw dislocation in c).

field. It was for example shown that an external field of 50 Oe, applied along the easy axis (along the long axis of the Fe-whisker), could move a 180° domain wall of an Fe-whisker (50 μm width) about 15 μm [48].

On the one hand, Fe-whiskers have flat and crystalline sample surfaces showing simple domain patterns. These advantages make Fe-whiskers attractive using them as test samples for measuring a well-defined in-plane component with our Sp-STM. On the other hand, they are small which is a problem when fixing them to a sample holder without producing a lot of external stress that modifies their domain pattern.

3.2.1 Preparation and characterization of the samples

The Fe-whiskers were cleaned by cycles of Argon sputtering and annealing to 720 K. The kinetic energy of the Ar^+ ions was 2 keV and a flux of 0.3 μA mm^{-2} was measured on the sample plate. The sample surface was controlled with AES and LEED. The magnetic structure of the Fe-whiskers was imaged in situ with a Kerr-microscope. It is not sufficient to check the domain pattern before the Fe-whisker is put into the vacuum chamber, because sputtering and annealing procedures may

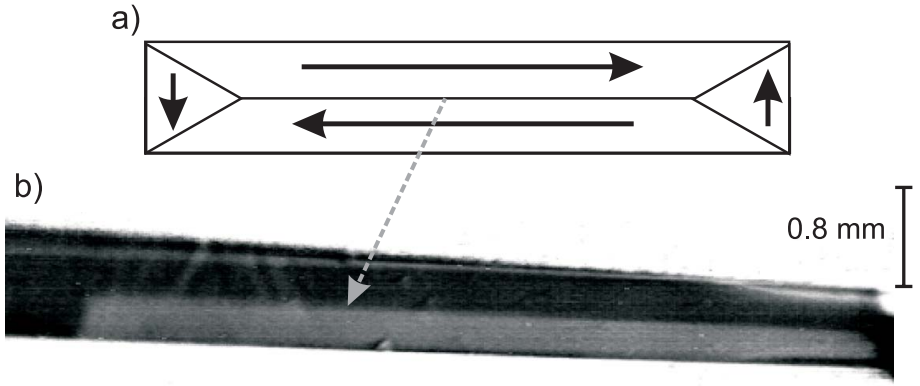

Figure 3.10: a) Schematic representation of a Landau-structure formed to minimize the stray field energy. The black arrows indicate the direction of the magnetization in each domain. b) Kerr-microscopy image of the surface of an Fe-whisker. Two domains are visible separated by a 180° domain wall along the long axis (the grey arrow indicates the correspondence between experiment and scheme). The structures at the ends are caused by stress due to the fixing of the Fe-whisker on a sample holder.

change these patterns.

Fig. 3.10b) shows an image of the domain configuration on a surface of an Fe-whisker taken with a Kerr-microscope. Two domains are visible separated by a 180° domain wall along the long axis. In the following experiments, the Fe-whiskers had such a domain configuration so that the direction of magnetization is well-defined and lies parallel to the long Fe-whisker axis.

3.2.2 Imaging of a 180° domain wall on an Fe-whisker

For Sp-STM measurements on Fe-whiskers, the direction of the ring and therefore the direction of spin sensitivity was chosen parallel to the long Fe-whisker axis. In Fig. 3.11a) and b) the topography and the spin signal is visible imaged with the Sp-STM on the surface of an Fe-whisker. The surface shows monatomic steps and terraces of 100 to 200 nm width. The corresponding spin signal in Fig. 3.11b) shows two areas of different spin signal represented as a black and white region. These correspond to two domains separated by a 180° domain wall running along the $\langle 100 \rangle$ direction. The difference in the spin signal between the two domains is 4%. This is a first proof that we are indeed able to image the in-plane spin polarization. In the spin signal, no crosstalk of the topography is seen and in the topography no influence of the magnetic domain wall is found.

Fig. 3.11c) shows a cross section of the calculated magnetic structure for a 180° domain wall in Fe near the surface [96]. The bulk Bloch wall, seen in the lower part of the figure rotates in the plane of the wall and terminates at the surface in a Néel cap. The calculations show that in this particular case the surface Néel wall is about

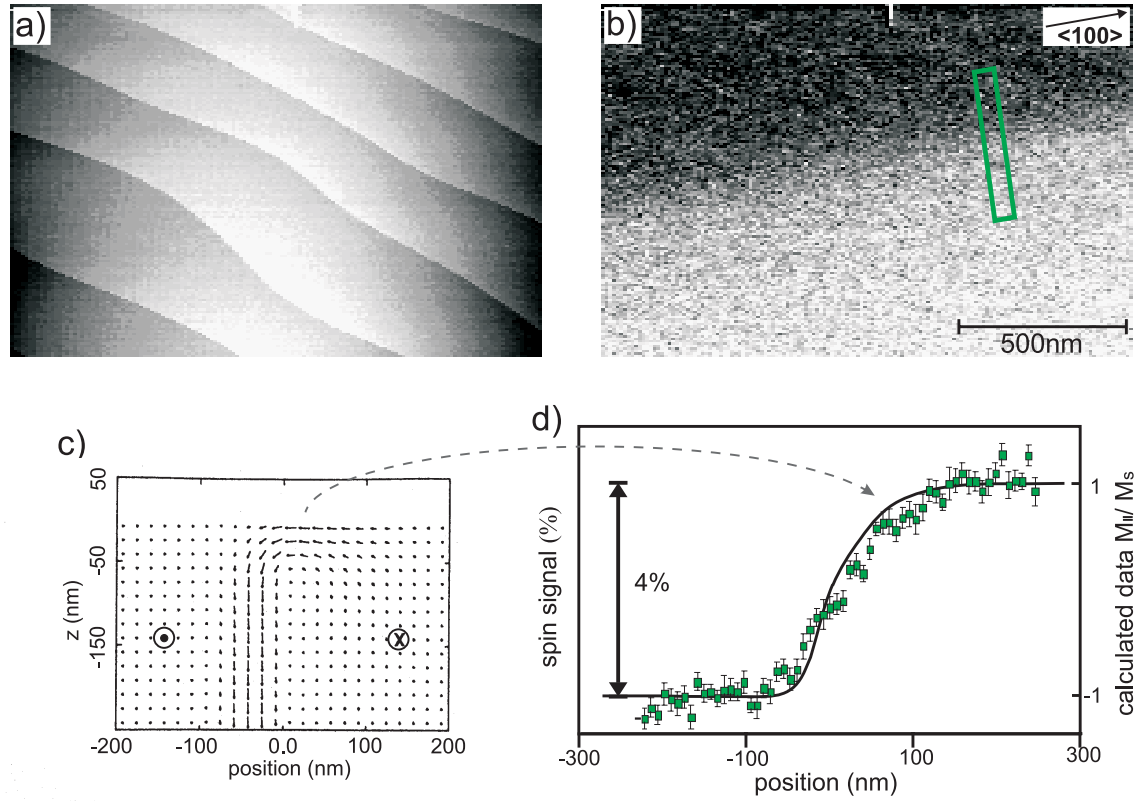

Figure 3.11: Sp-STM image of a) the topography and b) the spin signal of the surface of an Fe-whisker. Images were recorded simultaneously at a bias voltage of 0.4 V and a feedback current of 1 nA. c) Micromagnetic calculations of a 180° domain wall in Fe(001) [96]. The magnetization in the left and right part of the figure points out of and into the image plane, as indicated by the filled circles and the crosses. The arrows show the direction of the magnetization vector in the wall. d) Measured line profile (green squares and left scale) across the 180° domain wall at the position indicated by the green box in b). The error bars are the standard deviation of the mean value of 29 line scans. The black solid line represents the calculated line profile taken from c) (right scale) [96].

twice as wide as the bulk Bloch wall and penetrates into the crystal approximately by the width of the Bloch wall. Fig. 3.11d) shows a line profile over the measured 180° domain wall, obtained by averaging over 29 line scans (green squares). The line profile is taken at the position of the green box in Fig. 3.11b). The black solid line represents the micro-magnetically calculated surface line profile across the 180° domain wall, taken from the data in Fig. 3.11c) [96]. It shows the projection of the magnetization pointing along the domain boundary ($M_{\|}$) normalized to the saturation magnetization (M_s). A good agreement is found between the measured and calculated line profile within the lateral calibration error of the scanner ($\approx$ 10%). Néel caps create asymmetric walls [48] which are visible in the measured

and calculated line profile in Fig. 3.11d) so that a *tanh*-function does not fit the experimental wall profile satisfactory. Therefore, to extract the domain wall width we determined the intersection points of a tangent at the middle of the wall profile with a tangent of the maximum spin signal measured on both domains. This gives an estimate of the domain wall width of 150 nm. This is in good agreement with the width of 135±25 nm measured by Oepen and Kirschner [94] defined by the same procedure.

Such a good agreement is not always found. Some of the rings imaged slightly broader domain walls (some 50 nm) or even drag the walls some 100 nm. This might be due to the soft magnetic Fe-whisker where a 180° domain wall can be easily influenced by a small external field (see the introduction of Fe-whiskers in the beginning of this section). Likely, the occasional broadening and the dragging of walls is caused by a small residual stray field of the rings. By assuming a similar dependence of the movement of a 180° domain wall in an applied field as experimentally found by Hubert and Schäfer [48], the stray fields of the rings can be estimated to be of the order of 1 Oe.

The lateral resolution of the spin signal should be much better than the width of the imaged 180° domain wall. This is due to the fact that, as one can see from the topography, monatomic steps are resolved with a resolution of about 8 nm and the lateral resolution of the spin signal should be the same as the one of the topography. The resolution in this case is limited to the distance between two pixels. Because a large area was imaged the pixel density was low.

In conclusion, this experiment shows the first evidence that by Sp-STM measurements one well-defined in-plane component of the spin polarization of the sample surface can be imaged. Since the residual stray fields of the rings are small, even magnetic structures of soft magnetic materials can be imaged. The structure under investigation is well known and hence useful to test a new technique. However, the structure is big enough to be studied by other techniques. The real capability of the Sp-STM is to investigate magnetic structures on the nanometer scale. In the following chapter we focus on such small structures.